J Braz. Soc. Mech. Sci. Eng. (2017) 39:4519–4532
DOI 10.1007/s40430-017-0877-7

TECHNICAL PAPER

Influence of Stefan blowing on nanofluid flow submerged in microorganisms with leading edge accretion or ablation

Md. Faisal Md. Basir[1] · M. J. Uddin[2] · O. Anwar Bég[3] · A. I. Md. Ismail[1]

Received: 1 March 2017 / Accepted: 27 July 2017 / Published online: 7 August 2017

Abstract The forced convective boundary layer flow of viscous incompressible time-dependent fluid containing water-based nanofluids and gyrotactic microorganisms simultaneously, from a flat surface with leading edge accretion (or ablation), is theoretically investigated in the present study. In doing so, the governing conservation equations are rendered into a nonlinear system of ordinary differential equations by means of utilizing appropriate coordinates transformations. MAPLE symbolic software is employed to solve these equations, which are subjected to impose boundary conditions using the Runge–Kutta–Fehlberg fourth-fifth order numerical method. It is noteworthy that the results of the present study are in an excellent agreement with previous solutions available in literature. The effect of selected parameters on velocity, temperature, nanoparticle volume fraction and motile microorganism density function is then investigated. Tabular solutions are included for the skin friction, heat transfer rate, nano-particle mass transfer rate and microorganism transfer rate. Applications of the study arise in advanced micro-flow devices to bio-modified nanomaterials processing.

Technical Editor: Jader Barbosa Jr.

✉ Md. Faisal Md. Basir
faisalbasir91@gmail.com

M. J. Uddin
drjashim@aiub.edu

O. Anwar Bég
O.A.Beg@salford.ac.uk

A. I. Md. Ismail
ahmad_izani@usm.my

[1] School of Mathematical Sciences, University Sains Malaysia, 11800 Penang, Malaysia

[2] American International University-Bangladesh, Banani, Dhaka 1213, Bangladesh

[3] Aeronautical/Mechanical Engineering, University of Salford, Manchester M54WT, UK

Keywords Bioconvection · Nanofluids · Stefan blowing · Numerical solution · Accretion/ablation

List of symbols

$\tilde{b}$	Chemotaxis constant (m)
C	Nano-particles volume fraction $(-)$
C_{w}	Wall nano-particle volume fraction $(-)$
C_{∞}	Ambient nano-particle volume fraction $(-)$
$C_{\mathrm{f}_{\bar{x}}}$	Local skin friction coefficient along the $\bar{x}$ $(-)$
c_{p}	Specific heat at constant pressure $\left(\frac{\mathrm{J}}{\mathrm{kgK}}\right)$
D_{B}	Brownian diffusion coefficient $\left(\frac{\mathrm{m}^2}{\mathrm{S}}\right)$
D_n	Microorganism diffusion coefficient $\left(\frac{\mathrm{m}^2}{\mathrm{S}}\right)$
D_{T}	Thermophoresis diffusion coefficient $\left(\frac{\mathrm{m}^2}{\mathrm{S}}\right)$
$f(\eta)$	Dimensionless stream function $(-)$
$\vec{j}$	Vector flux of microorganisms $\left(\frac{\mathrm{kg}}{\mathrm{m}^2\mathrm{s}}\right)$
k	Thermal conductivity $\left(\frac{\mathrm{W}}{\mathrm{mK}}\right)$
Lb	Bioconvection Lewis number $\left(Lb = \frac{\alpha}{D_n}\right)$ $(-)$
Le	Lewis number $\left(Le = \frac{\alpha}{D_{\mathrm{B}}}\right)$ $(-)$
Nb	Brownian motion parameter $\left(Nb = \frac{\tau D_{\mathrm{B}}(C_{\mathrm{w}} - C_{\infty})}{\alpha}\right)$ $(-)$
$Nn_{\bar{x}}$	Local density number of motile microorganisms $(-)$

Nt	Thermophoresis parameter $\left(Nt = \frac{\tau D_T (T_w - T_\infty)}{\alpha T_\infty}\right)$ $(-)$
$Nu_{\bar{x}}$	Local Nusselt number $(-)$
n	Number of motile microorganisms $(-)$
n_w	Wall motile microorganisms $(-)$
Pe	Bioconvection Péclet number $\left(Pe = \frac{\tilde{b} W_c}{D_n}\right)$ $(-)$
Pr	Prandtl number $\left(Pr = \frac{\upsilon}{\alpha}\right)$ $(-)$
Re	Reynolds number $\left(\frac{\bar{U}_\infty \bar{x}}{\upsilon}\right)(-)$
$Sh_{\bar{x}}$	Local Sherwood number $(-)$
s	Wall mass flux (Stefan blowing)$\left(\frac{C_w - C_\infty}{1 - C_w}\right)(-)$
$\bar{t}$	Dimensional time (s)
T	Nanofluid temperature (K)
T_w	Wall temperature (K)
T_∞	Ambient temperature (K)
$\bar{U}_\infty$	Dimensional ambient velocity $\left(\frac{\mathrm{m}}{\mathrm{s}}\right)$
$\bar{u}$	Velocity components along the $\bar{x}$-axis $\left(\frac{\mathrm{m}}{\mathrm{s}}\right)$
$\vec{\bar{v}}$	Velocity vector $\left(\frac{\mathrm{m}}{\mathrm{s}}\right)$
$\tilde{\bar{v}}$	Average swimming velocity vector of microorganism $\left(\frac{\mathrm{m}^2}{\mathrm{s}}\right)$
$\bar{v}$	Velocity components along the $\bar{y}$-axis $\left(\frac{\mathrm{m}}{\mathrm{s}}\right)$
W_c	Maximum cell swimming speed $\left(\frac{\mathrm{m}}{\mathrm{s}}\right)$
$\bar{x}$	Dimensional coordinate along the surface (m)
$\bar{y}$	Coordinate normal to the surface (m)

Greek letters

α	Effective thermal diffusivity $\left(\frac{\mathrm{m}^2}{\mathrm{s}}\right)$
γ	Leading edge accretion/ablation $(-)$
η	Independent similarity variable $(-)$
$\theta(\eta)$	Dimensionless temperature $(-)$
μ	Dynamic viscosity $\left(\frac{\mathrm{kg}}{\mathrm{ms}}\right)$
υ	Kinematic viscosity $\left(\frac{\mathrm{m}^2}{\mathrm{s}}\right)$
ρ	Fluid density $\left(\frac{\mathrm{kg}}{\mathrm{m}^3}\right)$
π	Pi $(-)$
$(\rho c)_f$	Volumetric heat capacity of the fluid $\left(\frac{\mathrm{J}}{\mathrm{m}^3\mathrm{K}}\right)$
$(\rho c)_p$	Volumetric heat capacity of the nanoparticle material $\left(\frac{\mathrm{J}}{\mathrm{m}^3\mathrm{K}}\right)$
σ	Dimensionless time variable $\left(\bar{U}_\infty\, \bar{t}/\bar{x}\right)(-)$
τ	Ratio of the effective heat capacity of the nanoparticle material to the fluid heat capacity $\left(\frac{(\rho c)_p}{(\rho c)_f}\right)(-)$
$\phi(\eta)$	Dimensionless nanoparticles volume fraction $(-)$
$\chi(\eta)$	Dimensionless number of motile microorganisms $(-)$
ψ	Streamline function $(-)$

Subscripts

$(\ )'$	Ordinary differentiation with respect to η
$(\ )_w$	Condition at wall
$(\ )_\infty$	Condition in free stream

1 Introduction

The analysis of convective heat and mass transfer with nanoparticles has gained abundance of attention amongst researchers in recent years. Heat exchange may be increased by including nanofluids, which are the ultrafine particles with enhanced thermal properties in minimal volume fraction within the liquid that directs to modern class of fluids [1]. Traditional heat transfer fluids are regarded as poor heat transfer fluids, which include water, oil and ethylene glycol [2]. Many strategies have been used to enhance their thermal conductivity as the thermal conductivity of these liquids is regarded as a critical part in the heat transfer coefficient. It is now well known that a significant improvement in thermal conductivity can be obtained by adding nanometer-sized particles suspended in traditional heat transfer liquids. In this manner, nanomaterials are perceived to be more successful in smaller scale/nano electromechanical devices, advanced cooling frameworks, extensive scale thermal frameworks in evaporators, heat exchangers and mechanical cooling applications. Nanofluids are normally stable subject to a variety of operation conditions with no additional issues of disintegration, sedimentation, clogging, coagulation or extra weight drop. This is a direct result of the small size and low volume nano-particles required for thermal conductivity improvement [3]. The dissolving medium may be aqueous or non-aqueous in environment and nanoparticles may comprise metals, carbides, oxides, carbon nanotubes or nitrides. Shapes of the nanoparticles are: disks, spherical, cylindrical, etc. [4]. Recently, many studies of computational modeling of nanofluids have been communicated with diverse applications [5–17].

Bioconvection has important applications in bio-microsystems where it is utilized. For instance, to enhance mass transport, as well as to enhancement and mixing. When the spontaneous pattern formation and density stratification are caused by the simultaneous interaction of the denser self-propelled microorganisms, nanoparticles, and buoyancy forces (in the case of free convection), nano-bioconvection takes place [18]. Microorganisms have the tendency to swim in particular directions when responding to particular stimuli. These responses are known as taxes and the examples are gravitaxis, gyrotaxis, phototaxis, magneto-taxis and chemotaxis [19]. Gravitaxis means the swimming reverse to gravity and gyrotaxis is the swimming obtained the equilibrium of torques owing to viscous forces from shear flows. Phototaxis is due to the movement toward or away from light [20]. Analytical studies of nanofluid bioconvection were first presented by [21–27]. Makinde and Animasaun [28] reported that heat and mass transfer behavior decreases the diffusion of motile microorganisms. Akbar and Khan [29] studied the effects of magneto-bioconvection flow over a stretching sheet. Amirsom et al. [30] discussed the three-dimensional stagnation point flow of fluid involving both nanoparticles and gyrotactic microorganisms taking into account variable transport properties. Babu and Sandeep [31] simulated the non-aligned bioconvective flow of a nanofluid from a stretched sheet. Raees et al. [32] considered theoretically three-dimensional stagnation flow on a plate with anisotropic slip in a suspension of microorganisms and nanoparticles.

Far field as well as wall conditions are important in simulating nanocovetive transport problems. The blowing effect is originated from Stefan problem for species transfer [33]. In engineering applications, for example paper drying processes, mass transfer is obtained by evaporation [34]. A bulk motion of the fluid and extra-induced motion of the fluid are produced from the diffusion of the species [35]. In this study, the solid surface which is affected by the blowing is not considered to be porous. Further, the blowing is assumed to be due to flux transfer of species from the solid surface to outside/inside of the boundary layer. Species transfer varies on the flow field and the flow field is affected by the mass blowing at the wall. Fang and Jing [33] and Uddin et al. [36] investigated the boundary layer flow taking into account the Stefan blowing and have shown that the blowing velocity was directly proportional to the mass transfer flux.

In this present paper, we have employed the Buongiorno nanofluid model [37] which incorporates both thermophoretic and Brownian motion effects. The model has been successfully deployed by several authors [38–48].

An unsteady boundary layer model involving a moving leading edge exhibiting a certain rate of accretion or ablation was probably first introduced by Todd [49]. This problem is then stimulated considerable interest in recent years. Different velocity variation trends arise for different leading edge accretion/ablation effects; these can alter heat, mass and microorganism transfer rates within the respective boundary layers.

Analysis of boundary layers flow with accretion and ablation effects has been conducted by [50] and [2]. Recently, Rosca and Pop [51] have considered momentum, thermal and solutal boundary layer flows using the Buongiorno nanofluid model with accretion/ablation effects. The aim of this paper is to extend the work of the [2, 49–51], to the unsteady boundary layer flow of Buongiorno nanofluid by incorporating bioconvection phenomena.

2 Mathematical model

We consider two-dimensional, unsteady, incompressible, viscous, constant transport property, laminar forced convective flow of a nanofluid past a solid stationary semi-infinite plate with leading edge accretion/ablation. The nanofluid involves gyrotactic microorganisms. The influences of Stefan blowing are taken into account. Let the free stream velocity be $\bar{U}_\infty$, the free stream temperature be T_∞, the free stream nanoparticle volume flux as C_∞ and the free stream microorganism be zero $(n_\infty = 0)$. It also assumed that the uniform temperature, nanoparticle volume fraction and motile microorganism density at the plate are T_{w}, C_{w} and n_{w}, respectively. Let $(\bar{u}, \bar{v})$ and $(\bar{x}, \bar{y})$ be the dimensional velocity components in the vertically upward direction (parallel to the free stream) and perpendicular to the plate, respectively. The physical configuration of the problem is shown in Fig. 1, wherein (1) represents the momentum and (2) symbolize thermal, mass diffusion and microorganism boundary layers. Under above assumptions and following model equations proposed by [37] and [52], the vector field equations are:

$$\nabla \cdot \vec{v} = 0, \tag{1}$$

$$\frac{\partial \vec{v}}{\partial \bar{t}} + \left(\vec{v} \cdot \nabla\right)\vec{v} = -\frac{1}{\rho}\nabla p + \upsilon\, \nabla^2 \vec{v}, \tag{2}$$

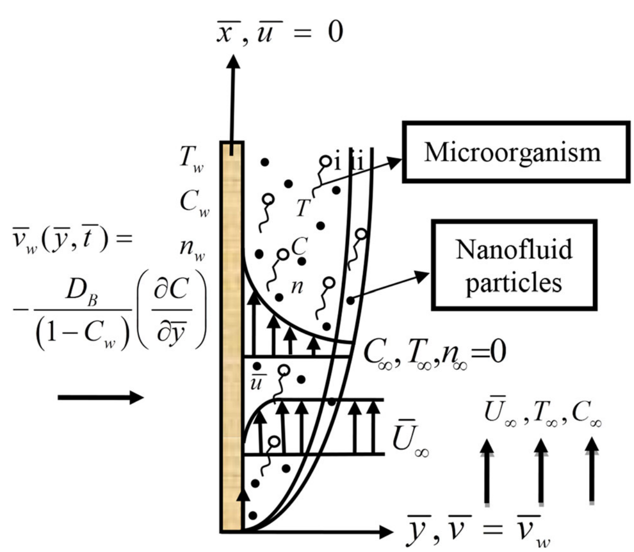

Fig. 1 Flow model and coordinate system

$$\frac{\partial T}{\partial \bar{t}} + (\vec{v}\cdot\nabla)T = \alpha\nabla^2 T + \tau\left[D_B\,\nabla T\cdot\nabla C + \left(\frac{D_T}{T_\infty}\right)\nabla T\cdot\nabla T\right] \tag{3}$$

$$\frac{\partial C}{\partial \bar{t}} + \left(\vec{v}\cdot\nabla\right)C = D_B\left(\nabla^2 C\right) + \left(\frac{D_T}{T_\infty}\right)\nabla^2 T, \tag{4}$$

$$\frac{\partial n}{\partial \bar{t}} + \nabla\cdot\vec{j} = 0, \tag{5}$$

where $\nabla = \frac{\partial}{\partial x}\vec{i} + \frac{\partial}{\partial y}\vec{j}$, ∇^2 is the Laplacian operator, υ is the kinematic viscosity,ρ is the fluid density, α is the thermal diffusivity of the fluid, $\tau = (\rho c)_p/(\rho c)_f$ is the ratio of effective heat capacity of the nanoparticle material to the fluid heat capacity, D_B is the Brownian diffusion coefficient, D_T is the thermophoretic diffusion coefficient and $\vec{j}$ is the flux of microorganisms that is defined as:

$$\vec{j} = n\,\vec{v} + n\,\tilde{\bar{v}} - D_n\,\nabla n, \tag{6}$$

In the Eq. (5), D_n is the diffusivity of microorganisms, $\tilde{\bar{v}} = \left(\frac{\tilde{b}W_c}{\Delta C}\right)\nabla C$ is the average swimming speed velocity vector of the gyrotactic microorganism, $\tilde{b}$ is the chemotaxis constant and W_c is the maximum cell swimming speed.

After using order of magnitude, the Eqs. (1)–(5) can be written in scalar form as:

$$\frac{\partial \bar{u}}{\partial \bar{x}} + \frac{\partial \bar{v}}{\partial \bar{y}} = 0, \tag{7}$$

$$\frac{\partial \bar{u}}{\partial \bar{t}} + \bar{u}\frac{\partial \bar{u}}{\partial \bar{x}} + \bar{v}\frac{\partial \bar{u}}{\partial \bar{y}} = \upsilon\frac{\partial^2 \bar{u}}{\partial \bar{y}^2} + \bar{u}_e\frac{\partial \bar{u}_e}{\partial \bar{x}} + \frac{\partial \bar{u}_e}{\partial \bar{t}}, \tag{8}$$

$$\frac{\partial T}{\partial \bar{t}} + \bar{u}\frac{\partial T}{\partial \bar{x}} + \bar{v}\frac{\partial T}{\partial \bar{y}} = \alpha\frac{\partial^2 T}{\partial \bar{y}^2} + \tau D_B\frac{\partial T}{\partial \bar{y}}\frac{\partial C}{\partial \bar{y}} + \tau\frac{D_T}{T_\infty}\left(\frac{\partial T}{\partial \bar{y}}\right)^2, \tag{9}$$

$$\frac{\partial C}{\partial \bar{t}} + \bar{u}\frac{\partial C}{\partial \bar{x}} + \bar{v}\frac{\partial C}{\partial \bar{y}} = D_B\frac{\partial^2 C}{\partial \bar{y}^2} + \frac{D_T}{T_\infty}\frac{\partial^2 T}{\partial \bar{y}^2}, \tag{10}$$

$$\frac{\partial n}{\partial \bar{t}} + \bar{u}\frac{\partial n}{\partial \bar{x}} + \bar{v}\frac{\partial n}{\partial \bar{y}} + \frac{\tilde{b}W_c}{C_w - C_\infty}\left[\frac{\partial}{\partial \bar{y}}\left(n\frac{\partial C}{\partial \bar{y}}\right)\right] = D_n\left(\frac{\partial^2 n}{\partial \bar{y}^2}\right), \tag{11}$$

subject to the following boundary conditions [36]:

$$\bar{u} = 0,\ \ \bar{v} = -\frac{D_B}{(1 - C_w)}\left(\frac{\partial C}{\partial \bar{y}}\right),\ T = T_w,\ C = C_w,\ n = n_w \ \text{as}\ \bar{y} = 0,$$
$$\bar{u} = \bar{u}_e = \bar{U}_\infty,\quad T \to T_\infty,\ \ C \to C_\infty,\ \ n \to 0\ \ \text{as}\ \ \bar{y} \to \infty, \tag{12}$$

where the following notation applies—$\bar{u}_e$ is the external velocity, υ is the kinematic viscosity, and ρ is the fluid density.

We implement the following modified dimensional stream function, which incorporates ablation/accretion effects at the boundary layer leading edge:

$$\psi(\bar{x},\bar{y},\bar{t}) = \bar{U}_\infty\sqrt{\upsilon\bar{t}\cos\gamma + (\upsilon\bar{x}/\bar{U}_\infty)\sin\gamma}\,f(\eta) \tag{13}$$

Defining the coordinate transformation:

$$\eta = \bar{y}\Big/\sqrt{\upsilon\bar{t}\cos\gamma + (\upsilon\bar{x}/\bar{U}_\infty)\sin\gamma}, \tag{14}$$

Dimensionless temperature, nanoparticle volume fraction and microorganism density functions are defined as follows:

$$\theta(\eta) = (T - T_\infty)/(T_w - T_\infty),\quad \phi(\eta) = (C - C_\infty)/(C_w - C_\infty),\quad \chi(\eta) = n/n_w. \tag{15}$$

Here, the dimensionless variables are η (similarity), $f'(\eta)$ (velocity), $\theta(\eta)$(temperature), $\phi(\eta)$(nanoparticle volume fraction), $\chi(\eta)$(microorganisms), γ is the leading edge accretion/ablation parameter and $\bar{t}$ is the dimensional time. Subscripts w and ∞ denote at the wall and in the free stream, respectively. Prime denotes ordinary differentiation with respect to η. The quantity $(\upsilon\bar{t}\cos\gamma + (\upsilon\bar{x}/\bar{U}_\infty)\sin\gamma)$ must be positive [49]. $\psi(\bar{x},\bar{y},\bar{t})$ is the streamline function, which is defined as:

$$\bar{u} = \partial\psi/\partial\bar{y}\ \text{and}\ \bar{v} = -\partial\psi/\partial\bar{x}. \tag{16}$$

Substituting Eqs. (13) and (14) into Eq. (16), we obtain $\bar{u}$ and $\bar{v}$ as follows:

$$\bar{u} = \bar{U}_\infty f',\quad \bar{v} = \frac{\upsilon}{2}(\eta f' - f)\sin\gamma\Big/\sqrt{\upsilon\bar{t}\cos\gamma + (\upsilon\bar{x}/\bar{U}_\infty)\sin\gamma}, \tag{17}$$

Proceeding with the analysis, the primitive partial differential conservation equations Eqs. (8)–(11) may be transformed into the following system of nonlinear similarity ordinary differential equations as follows:

$$f''' + \frac{1}{2}(\sin\,\gamma)ff'' + \frac{1}{2}(\cos\,\gamma)\eta f'' = 0, \tag{18}$$

$$\theta'' + \frac{1}{2}Pr\,(\eta\cos\,\gamma + f\,\sin\,\gamma)\,\theta' + Nb\,\theta'\,\phi' + Nt\,\theta'^2 = 0, \tag{19}$$

$$\phi'' + \frac{1}{2}Le\,Pr\,(\eta\cos\,\gamma + f\,\sin\,\gamma)\,\phi' + \frac{Nt}{Nb}\theta'' = 0, \tag{20}$$

$$\chi'' + \frac{1}{2}Pr\,Lb\,(\eta\cos\,\gamma + f\,\sin\,\gamma)\chi' - Pe[\chi\,\phi'' + \phi'\chi'] = 0, \tag{21}$$

The transformed associated boundary conditions emerge as follows:

$$f(0) = \frac{2}{Pr\,Le}\frac{1}{\sin\gamma}s\,\phi',\ f'(0) = 0,\ \theta(0) = 1,\ \ \phi(0) = 1,$$
$$\chi(0) = 1, f'(\infty) = 1,\ \ \theta(\infty) = \phi(\infty) = \chi(\infty) = 0, \tag{22}$$

where the following dimensionless parameters arise: Prandtl number (*Pr*), Lewis number (*Le*), Brownian motion parameter (*Nb*), thermophoresis parameter (*Nt*), bioconvection Lewis number (*Lb*), bioconvection Péclet number (*Pe*) and the mass blowing/suction parameter (Stefan blowing) (*s*). These parameters are defined, respectively, as:

$$Pr = \upsilon/\alpha,\ Nb = \tau D_{\mathrm{B}}(C_{\mathrm{w}} - C_\infty)/\alpha,\ Le = \alpha/D_{\mathrm{B}},$$
$$Nt = \tau D_{\mathrm{T}}(T_{\mathrm{w}} - T_\infty)/\alpha T_\infty, Lb = \alpha/D_n,\ Pe = \tilde{b}W_{\mathrm{c}}/D_n,$$
$$s = (C_{\mathrm{w}} - C_\infty)/(1 - C_{\mathrm{w}}) \tag{23}$$

3 Physical quantities

In practical applications, the gradients of the velocity, temperature, nanoparticle species concentration and microorganism density function are required. These take the form of the local skin friction coefficient $C_{\mathrm{f}_{\bar{x}}}$, the local Nusselt number $Nu_{\bar{x}}$, the local Sherwood number $Sh_{\bar{x}}$ and the local density number of motile microorganisms $Nn_{\bar{x}}$, which may be defined as:

$$C_{\mathrm{f}_{\bar{x}}} = \frac{\mu}{\rho \bar{U}_\infty^2}\left(\frac{\partial \bar{u}}{\partial \bar{y}}\right)_{\bar{y}=0},\ Nu_{\bar{x}} = \frac{-\bar{x}}{(T_{\mathrm{w}} - T_\infty)}\left(\frac{\partial T}{\partial \bar{y}}\right)_{\bar{y}=0},$$
$$Sh_{\bar{x}} = \frac{-\bar{x}}{(C_{\mathrm{w}} - C_\infty)}\left(\frac{\partial C}{\partial \bar{y}}\right)_{\bar{y}=0},\ Nn_{\bar{x}} = \frac{-\bar{x}}{n_{\mathrm{w}}}\left(\frac{\partial n}{\partial \bar{y}}\right)_{\bar{y}=0}, \tag{24}$$

Employing Eqs. (13)–(17) and (24), the parameters may be re-formulated in terms of the similarity variables, as follows:

$$Re_{\bar{x}}^{1/2} C_{\mathrm{f}_{\bar{x}}} \sqrt{\sigma\cos\gamma + \sin\gamma} = f''(0),$$
$$Re_{\bar{x}}^{-1/2} Nu_{\bar{x}} \sqrt{\sigma\cos\gamma + \sin\gamma} = -\theta'(0),$$
$$Re_{\bar{x}}^{-1/2} Sh_{\bar{x}} \sqrt{\sigma\cos\gamma + \sin\gamma} = -\phi'(0)$$
$$Re_{\bar{x}}^{-1/2} Nn_{\bar{x}} \sqrt{\sigma\cos\gamma + \sin\gamma} = -\chi'(0). \tag{25}$$

Here, $Re_{\bar{x}} = \bar{U}_\infty \bar{x}/\upsilon$ is the local Reynolds number and $\sigma = \bar{U}_\infty\,\bar{t}/\bar{x}$ denotes dimensionless time variable, introduced by [53].

Note that in the absence of the Eqs. (19)–(21), $s = 0$ (no suction/injection), the present model reduces to [49]. Also note that $s > 0$ for species transfer from the wall to the free stream (evaporation), while $s < 0$ for species transfer from the free stream to the wall (condensation).

4 Numerical solutions and validation

Closed form analytical solutions of Eqs. (18)–(21) with associated boundary conditions of Eq. (22) are extremely difficult if not intractable. A numerical procedure for solution of the two-point boundary value problem is, therefore, selected. We used the Runge–Kutta–Fehlberg fourth-fifth order numerical method algorithm available in the symbolic code, Maple 2016 [54]. Comparison is also made with previously published results (Todd [49] and Rosca and Pop [51]), for local skin friction for several values of the accretion/ablation parameter (γ) as shown in Table 1. An excellent agreement is achieved and confidence in the present MAPLE solutions is, therefore, justifiably high.

5 Results and discussion

Extensive numerical solutions are presented graphically in Figs. 2, 3, 4, 5, 6, 7, 8, 9, 10 and 11, for the influence of parameters on the dimensionless velocity, temperature, nanoparticles volume fraction and microorganisms. Data have been selected where possible from existing references, e.g., ([49]). We have additionally computed the physical quantities. In the current simulations, Prandtl number (*Pr*) is prescribed as 6.8 (water-based nanofluid), for which it is known that gyrotactic microorganisms can thrive and remain active [55].

Figure 2a–d shows the effect of the Stefan blowing (s) and leading edge accretion/ablation (γ) on the dimensionless velocity, temperature, nanoparticle volume fraction and motile microorganism density function profiles. The dimensionless velocity significantly increases with negative Stefan blowing parameter ($s < 0$). Normally, with suction at the surface ($s = -1$), the bionanofluid is drawn

Table 1 Comparison of the values of the local skin friction coefficient $f''(0)$ for different values of accretion/ablation parameter (γ)

γ	$f''(0)$ Rosca and Pop [51]	$f''(0)$ Todd [49]	$f''(0)$ (MAPLE)
0	0.56418	0.5642	0.563751
$\pi/24$	0.57501	0.5750	0.574585
$\pi/12$	0.58072	0.5807	0.580381
$\pi/6$	0.57700	0.5770	0.576857
$\pi/4$	0.55287	0.5529	0.552780
$\pi/3$	0.50721	0.5072	0.507214
$5\pi/12$	0.43686	0.4369	0.436849
$11\pi/24$	0.38999	0.3900	0.389999
$\pi/2$	0.33205	0.3321	0.332051

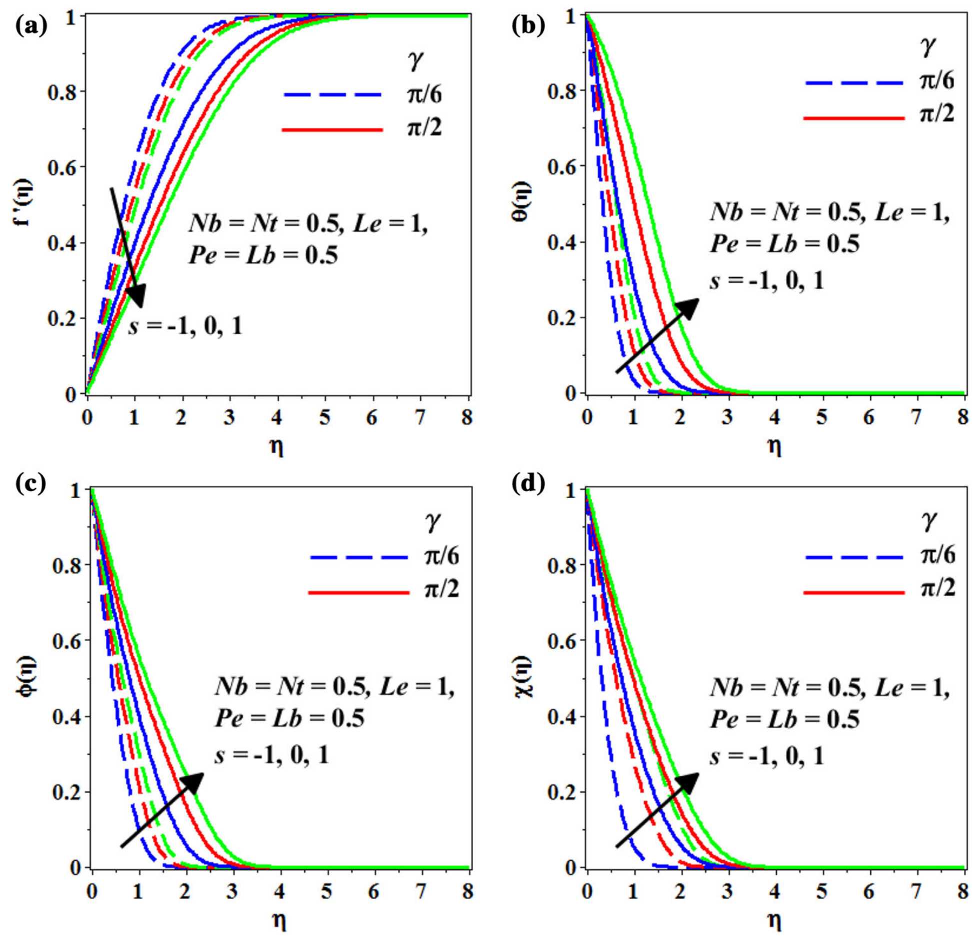

Fig. 2 Variation of $f'(\eta)$, $\theta(\eta)$, $\phi(\eta)$ and $\chi(\eta)$ with different values of γ and s

through the surface via apertures and this inhibits momentum transfer into the boundary layer by assisting adhesion of the boundary layer to the surface. As a result, the flow is decelerated strongly and this leads to an increase in thickness of the momentum boundary layer. With stronger blowing ($s = 1$), the hot nanofluid is displaced further from the surface where the buoyancy forces accelerate the flow. This effect enhances the shearing effect by increasing the maximum velocity within the boundary layer. The velocity profiles, therefore, are discrete for suction ($s = -1$) and injection ($s = 1$). An increase in the accretion/ablation effect ($\gamma > 0$) at the leading edge manifests in a deceleration in the flow, i.e., reduction in velocities. The case of $\gamma < 0$, which corresponds to backward flow with trailing edge accretion, is not considered. Momentum boundary layer thickness is increased with $\gamma > 0$. With greater suction ($s = -1$), temperatures are reduced and with greater injection ($s = 1$) they increase. Thermal boundary layer thickness is, therefore, greatest with mass injection into the boundary layer. The intermediate case of $s = 0$ corresponds to a solid (impermeable) wall. With increasing positive accretion/ablation rate ($\gamma > 0$), temperatures are strongly enhanced and thermal boundary layer thickness is elevated. The thermal field, therefore, responds very differently to leading edge accretion/ablation compared with the velocity field. With strong wall suction ($s = -1$) the nanoparticle concentration (volume fraction) decreases continuously throughout the boundary layer. Conversely with strong blowing ($s = 1$), nanoparticle concentration values are enhanced. The injection of nanofluid via the wall encourages species diffusion throughout the regime, whereas removal of nanofluid inhibits species (nanoparticle) diffusion. Increasing blowing, therefore, thickens the concentration boundary layer whereas increased suction has the adverse effect. Increased accretion/ablation ($\gamma > 0$) at the leading edge also exerts a similar effect on nanoparticle volume fraction to that on the temperature distribution. It enhances nanoparticle concentration magnitudes consistently from the wall to the free stream. Greater injection is also observed to elevate microorganism density function (Fig. 2d), whereas stronger suction induces the reverse effect and suppresses microorganism density function. The transport of microorganisms is, therefore, encouraged with blowing through the wall and the corresponding boundary layer thickness is elevated. Increasing accretion/ablation

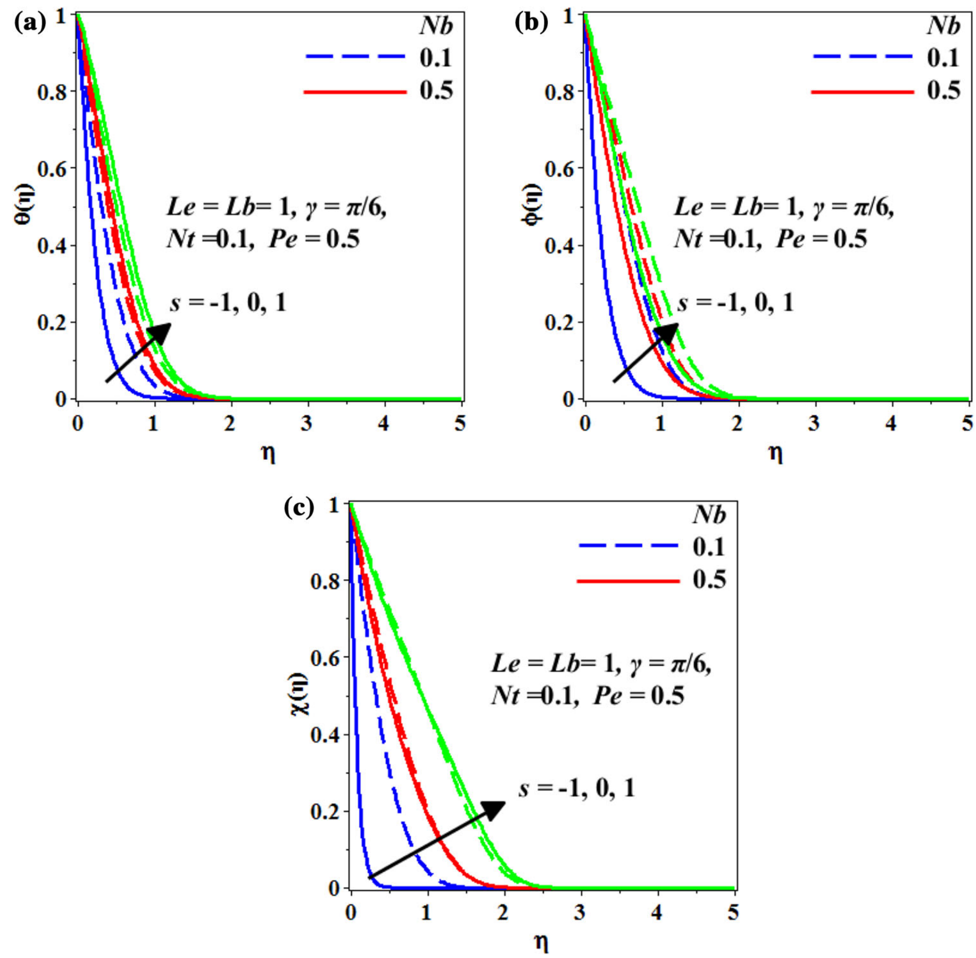

Fig. 3 Variation of $\theta(\eta)$, $\phi(\eta)$ and $\chi(\eta)$ with different values of *Nb* and *s*

also enhances microorganism density function values. It is worth highlighting that the present analysis found that the movement of the motile microorganisms is independent of the motion of nanoparticles. The nanoparticles are transported via Brownian motion and by not self-propulsion as with microorganisms.

Figure 3a–c presents the distribution of temperature, nanoparticle volume fraction and microorganism, respectively, for different values of the Brownian motion parameter (*Nb*) and the suction/blowing parameter (*s*). In these figures, again, we consider leading edge accretion/ablation to be present with γ prescribed as $\pi/6$. An elevation in Brownian motion parameter physically correlates with smaller nanoparticles diameters, based on the Buongiorno formulation employed in the present model. For solid wall case or injection ($s > 0$), larger *Nb* values (smaller sized nanoparticles) result in enhanced thermal conduction and this, in turn, increases nanofluid temperatures. Conversely, smaller *Nb* values correspond to large nanoparticles which serve to inhibit thermal conduction and decrease temperatures in the nanofluid and, therefore, reduce the thermal boundary layer thickness. The boost in temperatures with smaller nanoparticles, in which the heat diffuses faster in nanofluids compared to vorticity. Hence, this implies a deceleration in the flow with greater Brownian motion effect, although velocity plots have been omitted for brevity. Nanoparticle concentration (Fig. 3b) is observed to be suppressed with increasing Brownian motion parameter, i.e., concentration boundary layer thickness decreases with larger value of *Nb*. With greater wall suction, both nanoparticle concentration (volume fraction) and also species boundary layer thickness are also decreased. The reverse effect is generated with wall blowing. The motile microorganism density function (Fig. 3c) also decreases with increasing Brownian motion parameter. Additionally with greater wall suction, nanofluids are removed from the boundary layer regime, and this reduces the motile microorganism density. With greater wall injection, the flow is accelerated and this enhances motile microorganism density function values, i.e., increases the concentration of gyrotactic microorganisms throughout the boundary layer regime.

Figure 4a–c depicts the velocity and temperature response with the combined effects of lateral mass flux

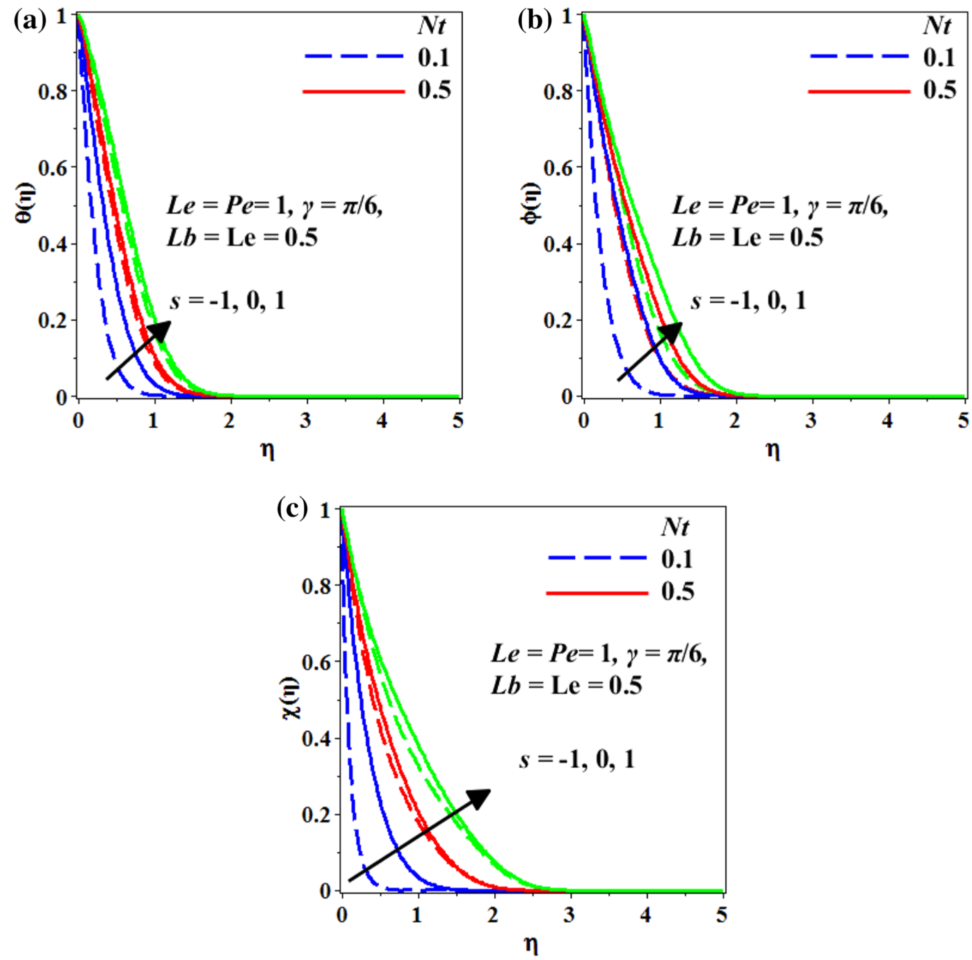

Fig. 4 Variation of $\theta(\eta)$, $\phi(\eta)$ and $\chi(\eta)$ with different values of *Nt* and *s*

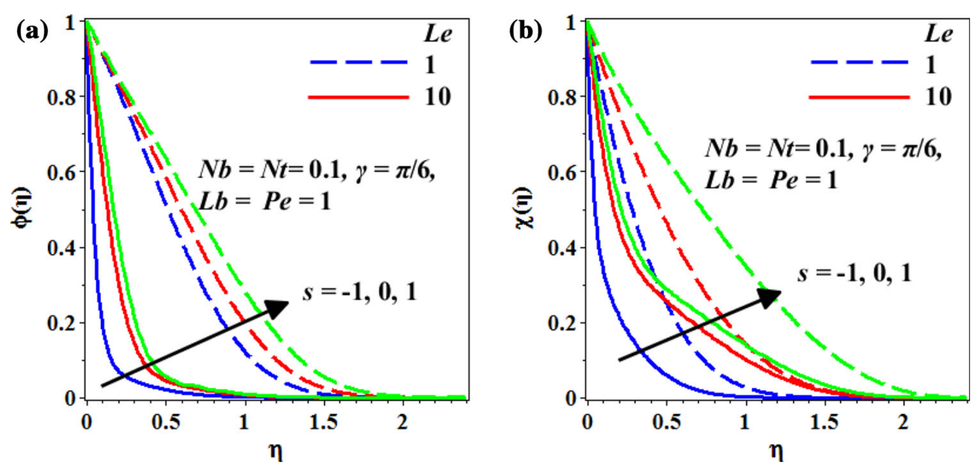

Fig. 5 Variation of $\phi(\eta)$ and $\chi(\eta)$ with different values of *Le* and *s*

(wall suction or blowing) parameter (*s*) and the thermophoresis parameter (*Nt*). A growth in *Nt* also induces a boost in temperatures. Thermophoretic migration of nanoparticles encourages thermal diffusion in the regime and energizes the flow. This enhances temperatures, i.e., heats the nanofluid and increases thermal boundary layer thickness. Figure 4b also shows that a rise in nanoparticle volume fraction, $\phi(\eta)$, accompanies a larger injection. Scrutiny of Fig. 4c reveals that with stronger blowing and *Nt* values, diffusion of motile microorganisms is encouraged and a substantial increase in magnitudes of motile density function is produced. The converse response is computed for stronger suction.

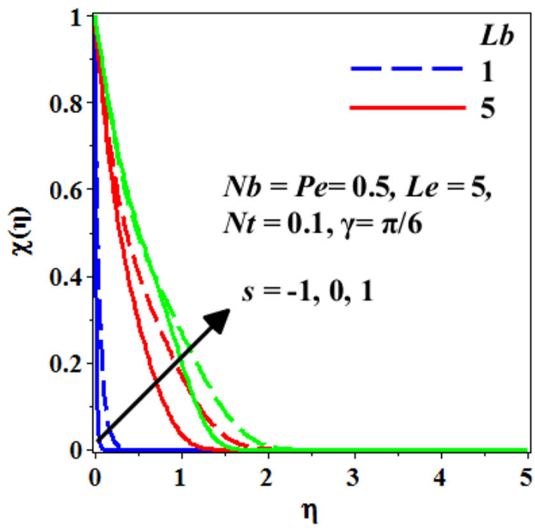

Fig. 6 Variation of $\chi(\eta)$ with different values of *Lb* and *s*

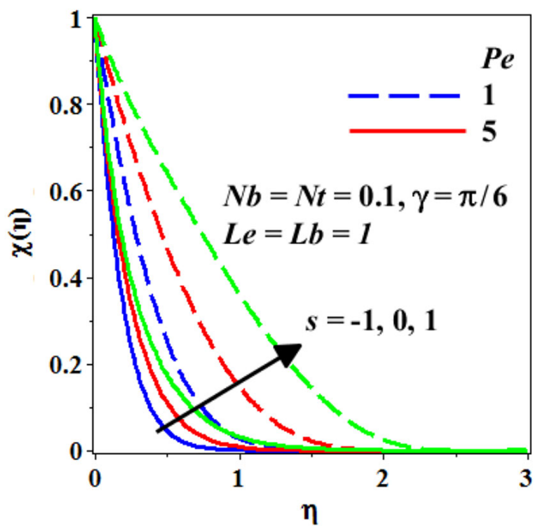

Fig. 7 Variation of $\chi(\eta)$ with different values of *Pe* and *s*

Figure 5a, b shows the effect of the conventional Lewis number (*Le*) on nanoparticle and microorganism species diffusion characteristics. *Le* is the ratio of the thermal diffusivity to the nanoparticle species diffusivity. When $Le = 1$ the heat diffusion and nanoparticle diffusion rates are equal and thermal and nanoparticle boundary layer thicknesses will be equivalent. For $Le > 1$, heat diffuses faster than nanoparticle species. This reduces the efficiency of the nanoparticle migration in the nanofluid. Nanoparticle concentrations are lowest (Fig. 5a) with greater Lewis number and strong wall suction present. Increasing Lewis number results in a depression in microorganism density function (concentration) magnitudes. The highest values of the microorganism density function are achieved with strong injection and the lowest magnitudes correspond to strong suction, at both values of the Lewis number.

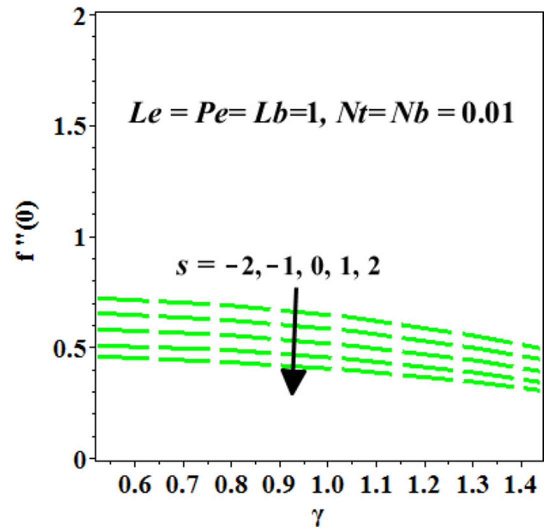

Fig. 8 Effect of *s* on $f''(0)$ with different values of γ

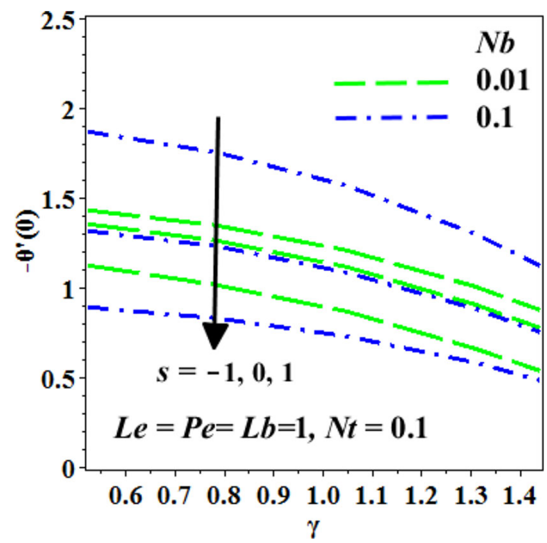

Fig. 9 Effect of *s* and *Nb* on $-\theta'(0)$ with different values of γ

Figure 6 visualizes the effect of bioconvection Lewis number (*Lb*) on the dimensionless microorganism density function. Traditional Lewis number is taken to be 5, i.e., the thermal diffusion rate is five times the nanoparticle diffusion rate. For *Lb* greater that unity, the thermal diffusion rate exceeds motile microorganism diffusion rate. Microorganism density is enhanced with a decrease in bioconvection Lewis number. The propulsion of motile microorganisms is increased and a more even distribution through the boundary layer is observed with higher microorganism diffusivity rates (Fig. 6). In this figure, it can be found that wall injection always achieves higher magnitudes of microorganism density function than wall suction.

Figure 7 presents the effect of the bioconvection Peclet number (*Pe*) on microorganism density. Bioconvection

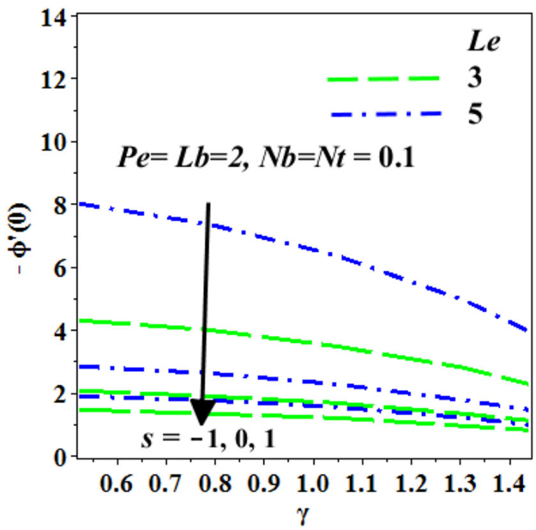

Fig. 10 Effect of s and Le on $-\phi'(0)$ with different values of γ

Peclét number is the ratio of advection rate of nanoparticles to the diffusion rate. $Pe < 10$ is more appropriate for actual transport phenomena in bioconvection nanofluid mechanics. Pe features only in the microorganism density conservation Eq. (21) via the coupling terms $-Pe\,[\chi\phi'' + \phi'\chi']$, which effectively links the nanoparticle concentration, and microorganism fields. These terms apparently have a pronounced influence on the evolution of microorganism density function. Bioconvection is generated from internal energy of the microorganisms. The microorganisms propel faster with greater swimming speed (higher bioconvection Peclet number) and, thus, reduce their concentrations, i.e., density function. Apart from that, it was revealed that injection can boost the concentration magnitudes of the microorganism, whereas suction may lead to reduction.

Figure 8 and Table 2 illustrate the collective effects of leading edge accretion/ablation parameter (γ) and wall mass flux (s) parameters on wall skin friction (surface shear stress function). Increasing the leading edge accretion/ablation parameter substantially reduces skin friction for any value of s. However, greater values are computed when wall suction is present ($s < 0$) compared to when wall blowing is present ($s > 0$). The boundary layer flow is clearly decelerated with greater leading edge accretion/ablation effect ($\gamma > 0$).

Table 2 Values of $f''(0)$ when $Nt = Nb = 0.01,\ Lb = Pe = Le = 1$

γ	$f''(0)$				
	$s=-2$	$s=-1$	$s=0$	$s=1$	$s=2$
$\pi/6$	0.720557	0.650015	0.577003	0.508971	0.454212
$\pi/4$	0.691224	0.623326	0.552876	0.487366	0.434987
$\pi/3$	0.635321	0.572555	0.507223	0.446679	0.398731
$5\pi/12$	0.549287	0.494352	0.436897	0.384044	0.342919
$11\pi/24$	0.492358	0.442474	0.390113	0.342354	0.305825

Figure 9 and Table 3 show the response in wall heat transfer rate (temperature gradient) with different values of leading edge accretion/ablation parameter (γ), Brownian motion parameter (Nb) and wall mass flux parameter (s). Increasing leading edge accretion/ablation strongly reduces the wall heat transfer rate both with wall suction and blowing. With increasing Brownian motion effect (higher Nb values), the nanoparticles are reduced in size. This decreases the heat transfer rate to the wall since greater temperatures are induced in the body of the fluid with smaller nanoparticles and thermal energy is retained in the fluid with lower transport rates to the wall. The opposite effect is apparent with smaller Nb values, which imply larger nanoparticles, lower temperatures and, therefore, higher heat transfer rates to the wall.

Figure 10 and Table 4 depict the effect of leading edge accretion/ablation parameter (γ), Lewis number (Le) and wall mass flux parameter (s) on nanoparticle mass transfer

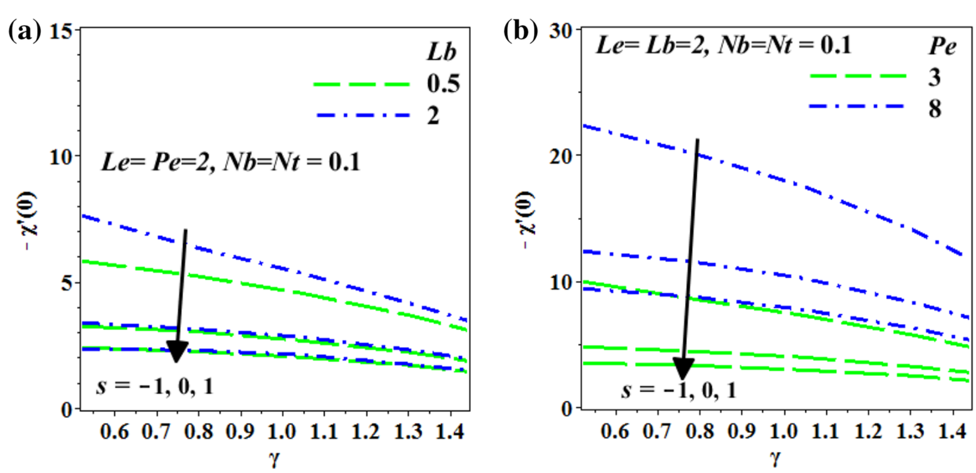

Fig. 11 Effect of s and γ on $-\chi'(0)$ with different values of **a** Lb and **b** Pe

Table 3 Values of $-\theta'(0)$ when $Nt = 0.1$, $Lb = Pe = Le = 1$

γ	$-\theta'(0)$					
	$Nb = 0.01$			$Nb = 0.1$		
	$s = -1$	$s = 0$	$s = 1$	$s = -1$	$s = 0$	$s = 1$
$\pi/6$	1.425487	1.349263	1.119020	1.868920	1.315193	0.893898
$\pi/4$	1.342286	1.258437	1.014321	1.754277	1.226549	0.827925
$\pi/3$	1.205121	1.114820	0.864940	1.567688	1.086215	0.726301
$5\pi/12$	1.005496	0.908305	0.661985	1.295692	0.883449	0.581199
$11\pi/24$	0.876657	0.774474	0.535403	1.117525	0.750455	0.486465

Table 4 Values of $-\phi'(0)$ when $Nb = Nt = 0.1$, $Lb = Pe = 2$

γ	$-\phi'(0)$					
	$Le = 3$			$Le = 5$		
	$s = -1$	$s = 0$	$s = -1$	$s = -1$	$s = 0$	$s = 1$
$\pi/6$	4.306463	2.048079	1.446564	7.998281	2.820157	1.903162
$\pi/4$	3.984718	1.897993	1.341580	7.348601	2.597780	1.754896
$\pi/3$	3.487046	1.665209	1.178481	6.359849	2.258300	1.528157
$5\pi/12$	2.769586	1.330258	0.943916	4.933065	1.770857	1.202951
$11\pi/24$	2.293186	1.109224	0.789474	3.971864	1.447093	0.987767

rate at the wall. Evidently, nanoparticle wall mass transfer rate is significantly greater with wall suction ($s < 0$) compared with wall blowing ($s > 0$), implying that destruction of fluid momentum encourages nanoparticle diffusion at the wall. With greater positive values of leading edge accretion/ablation parameter, nanoparticle wall mass transfer rate, $-\phi'(0)$ function values strongly decrease whereas with an increase in Lewis number they are markedly enhanced.

Finally, Fig. 11a, b, Tables 5 and 6 present the effects of different bioconvection parameters (bioconvection Lewis number and Péclet number, i.e., *Lb* and *Pe,* respectively) on the motile microorganism wall mass transfer rate, $-\chi'(0)$. In Fig. 11a, increasing bioconvection Lewis number (*Lb*) significantly enhances the motile microorganism wall mass transfer rate irrespective of whether blowing or suction is present. With increasing leading edge accretion/ablation parameter, motile microorganism wall mass transfer rate is depressed for the case of wall injection ($s < 0$) and elevated with wall suction ($s > 0$). In Fig. 11b, with greater bioconvection Péclet number, there is a strong increment in the motile microorganism wall mass transfer rate with either suction or injection present, although magnitudes are much reduced with larger values of accretion/ablation parameter.

6 Conclusions

A theoretical study has been conducted to simulate two-dimensional, unsteady, laminar, incompressible, gyrotactic bioconvection nanofluid boundary layer flow from a plane surface with leading accretion/ablation. Wall mass flux (Stefan blowing or suction) effects have also been incorporated in the model via the boundary conditions at the wall. The transformed similarity ordinary differential equations have been solved with Maple symbolic software using RKF45 quadrature with a shooting algorithm. Very close agreement with previously published solutions has been obtained. The influence of leading edge accretion/ablation, bioconvection (bioconvection Lewis number and Péclet number), wall mass flux and nanoscale parameters on the dimensionless velocity, skin friction factor, temperature, wall heat transfer rate, nanoparticle concentration, nanoparticle wall mass transfer rate, motile microorganism density number function and wall microorganism mass transfer rate has been studied in detail. The present computations have shown that:

1. An increase in the accretion/ablation effect ($\gamma > 0$) at the leading edge decelerates the boundary layer flow, i.e., reduces velocity and skin friction but increases momentum boundary layer thickness.

Table 5 Values of $-\chi'(0)$ when $Nt = Nb = 0.1$, $Pe = Le = 2$

γ	$-\chi'(0)$					
	$Lb = 0.5$			$Lb = 2$		
	-1	0	1	-1	0	1
$\pi/6$	5.840798	3.232983	2.385871	7.621526	3.351096	2.341084
$\pi/4$	5.252215	3.023618	2.261013	6.398876	3.138006	2.291537
$\pi/3$	4.562483	2.689649	2.027465	5.328916	2.797387	2.089943
$5\pi/12$	3.665373	2.204979	1.674657	4.145867	2.301754	1.750409
$11\pi/24$	3.098377	1.886119	1.439424	3.451491	1.974589	1.515804

Table 6 Values of $-\chi'(0)$ when $Nt = Nb = 0.1$, $Lb = Le = 2$

γ	$-\chi'(0)$					
	$Pe = 3$			$Pe = 8$		
	-1	0	1	-1	0	1
$\pi/6$	9.986980	4.766449	3.480706	22.302116	12.342187	9.435950
$\pi/4$	8.607940	4.453843	3.313131	20.132746	11.515440	8.756513
$\pi/3$	7.282920	3.956611	2.972202	17.504888	10.203930	7.739319
$5\pi/12$	5.726681	3.235709	2.450701	14.037149	8.306593	6.293144
$11\pi/24$	4.785869	2.761285	2.101388	11.832668	7.060678	5.349604

2. With increasing positive accretion/ablation rate ($\gamma > 0$), temperature, nanoparticle concentration (volume fraction) and microorganism density function are increased, as are the associated boundary layer thicknesses.
3. Temperature, nanoparticle concentration (volume fraction) and microorganism density function are decreased with stronger wall suction ($s = -1$), and enhanced with greater wall injection ($s = 1$).
4. With greater bioconvection Peclét number (Pe), microorganism density function is reduced.
5. With larger bioconvection Lewis number (Lb), the motile microorganism wall mass transfer rate is enhanced.
6. With increasing leading edge accretion/ablation parameter, motile microorganism wall mass transfer rate is reduced for wall injection ($s < 0$) and enhanced for wall suction ($s > 0$).
7. With higher values of leading edge accretion/ablation parameter, nanoparticle wall mass transfer rate is suppressed whereas with an increase in ordinary Lewis number it is elevated.
8. With increasing leading edge accretion/ablation parameter ($\gamma > 0$) and Brownian motion parameter (Nb), wall heat transfer rate (Nusselt number) is decreased.
9. An increase in thermophoresis parameter (Nt) elevates both temperature and thermal boundary layer thickness.

The present model has considered Newtonian nanofluids. Future investigations will address non-Newtonian bioconvection nanofluid flow in porous media considering gravitational forces and will be reported in due course. Moreover, the considered problem can be extended for convection through square enclosure enclosing (cavity) flow [56–58].

Acknowledgements The authors acknowledge financial support from Universiti Sains Malaysia, RU Grant 1001/PMATHS/8011013.

References

1. Choi SUS, Eastman JA (1995) Enhancing thermal conductivity of fluids with nanoparticles. ASME Int Mech Eng Congr Expo 66:99–105
2. Loganathan P, Vimala C (2014) Unsteady flow of nanofluids past a vertical flat plate with leading edge accretion or ablation. Indian J Phys 88:855–859
3. Hayat T, Imtiaz M, Alsaedi A (2016) Unsteady flow of nanofluid with double stratification and magnetohydrodynamics. Int J Heat Mass Transf 92:100–109
4. Shehzad N, Zeeshan A, Ellahi R, Vafai K (2016) Convective heat transfer of nanofluid in a wavy channel: Buongiorno's mathematical model. J Mol Liq 222:446–455

5. Malvandi A, Ghasemi A, Ganji DD (2016) Thermal performance analysis of hydromagnetic Al_2O_3-water nanofluid flows inside a concentric microannulus considering nanoparticle migration and asymmetric heating. Int J Therm Sci 109:10–22
6. Rahman MM, Alam MS, Eltayeb IA (2016) Hydromagnetic natural convective heat transfer flow in an isosceles triangular cavity filled with nanofluid using two-component nonhomogeneous model. Int J Therm Sci 107:272–288
7. Malvandi A, Moshizi SA, Ganji DD (2016) Effects of temperature-dependent thermophysical properties on nanoparticle migration at mixed convection of nanofluids in vertical microchannels. Powder Technol 303:7–19
8. Sheremet MA, Pop I, Roşca NC (2016) Magnetic field effect on the unsteady natural convection in a wavy-walled cavity filled with a nanofluid: Buongiorno's mathematical model. J Taiwan Inst Chem Eng 61:211–222
9. Akilu S, Sharma KV, Baheta AT, Mamat R (2016) A review of thermophysical properties of water based composite nanofluids. Renew Sustain Energy Rev 66:654–678
10. Ilhan B, Kurt M, Ertürk H (2016) Experimental investigation of heat transfer enhancement and viscosity change of hBN nanofluids. Exp Therm Fluid Sci 77:272–283
11. Agarwal R, Verma K, Kumar N, Singh R (2017) Sensitivity of thermal conductivity for Al_2O_3 nanofluids. Exp Therm Fluid Sci 80:19–26
12. Loganathan P, Chand PN, Ganesan P (2013) Radiation effects on an unsteady natural convective flow of a nanofluid past an infinite verticle plate. Nano 8:1–10
13. Mejri I, Mahmoudi A, Abbassi MA, Omri A (2014) Magnetic field effect on entropy generation in a nanofluid-filled enclosure with sinusoidal heating on both side walls. Powder Technol 266:340–353
14. Uddin MJ, Khan WA, Ismail AIM (2012) Lie group analysis of natural convective flow from a convectively heated upward facing radiating permeable horizontal plate in porous media filled with nanofluid. J Appl Math 2012:18. doi:10.1155/2012/648675
15. Hatami M, Sheikholeslami M, Ganji DD (2014) Laminar flow and heat transfer of nanofluid between contracting and rotating disks by least square method. Powder Technol 253:769–779
16. Freidoonimehr N, Rashidi MM, Mahmud S (2015) Unsteady MHD free convective flow past a permeable stretching vertical surface in a nano-fluid. Int J Therm Sci 87:136–145
17. Beg OA, Rashidi MM, Akbari M, Hosseini A (2014) Comparative numerical study of single-phase and two-phase models for bio-nanofluid transport phenomena. J Mech Med Biol 14:1450011
18. Mutuku WN, Makinde OD (2014) Hydromagnetic bioconvection of nanofluid over a permeable vertical plate due to gyrotactic microorganisms. Comput Fluids 95:88–97
19. Siddiqa S, Gul-e-Hina Begum N (2016) Numerical solutions of nanofluid bioconvection due to gyrotactic microorganisms along a vertical wavy cone. Int J Heat Mass Transf 101:608–613
20. Acharya N, Das K, Kumar P (2016) Framing the effects of solar radiation on magneto-hydrodynamics bioconvection nanofluid flow in presence of gyrotactic microorganisms. J Mol Liq 222:28–37
21. Kuznetsov AV (2006) The onset of thermo-bioconvection in a shallow fluid saturated porous layer heated from below in a suspension of oxytactic microorganisms. Eur J Mech B Fluids 25:223–233
22. Geng P, Kuznetsov AV (2004) Effect of small solid particles on the development of bioconvection plumes. Int Commun Heat Mass Transf 31:629–638
23. Kuznetsov AV, Nield DA (2014) Natural convective boundary-layer flow of a nanofluid past a vertical plate: a revised model. Int J Therm Sci 77:126–129
24. Kuznetsov AV (2012) Nanofluid bioconvection in a horizontal fluid-saturated porous layer. J Porous Media 15:11–27
25. Kuznetsov AV (2011) Bio-thermal convection induced by two different species of microorganisms. Int Commun Heat Mass Transf 38:548–553
26. Kuznetsov AV (2005) Thermo-bioconvection in a suspension of oxytactic bacteria. Int Commun Heat Mass Transf 32:991–999
27. Kuznetsov AV, Avramenko AA, Geng P (2004) Analytical investigation of a falling plume caused by bioconvection of oxytactic bacteria in a fluid saturated porous medium. Int J Eng Sci 42:557–569
28. Makinde OD, Animasaun IL (2016) Thermophoresis and Brownian motion effects on MHD bioconvection of nano fluid with nonlinear thermal radiation and quartic chemical reaction past an upper horizontal surface of a paraboloid of revolution. J Mol Liq 221:733–743
29. Akbar NS, Khan ZH (2016) Magnetic field analysis in a suspension of gyrotactic microorganisms and nanoparticles over a stretching surface. J Magn Magn Mater 410:72–80
30. Amirsom NA, Uddin MJ, Ismail AI (2016) Three dimensional stagnation point flow of bionanofluid with variable transport properties. Alex Eng J 55:1983–1993
31. Jayachandra Babu M, Sandeep N (2016) Effect of nonlinear thermal radiation on non-aligned bio-convective stagnation point flow of a magnetic-nanofluid over a stretching sheet. Alex Eng J 55:1931–1939
32. Raees A, Raees-ul-Haq M, Xu H, Sun Q (2016) Three-dimensional stagnation flow of a nanofluid containing both nanoparticles and microorganisms on a moving surface with anisotropic slip. Appl Math Model 40:4136–4150
33. Fang T, Jing W (2014) Flow, heat, and species transfer over a stretching plate considering coupled Stefan blowing effects from species transfer. Commun Nonlinear Sci Numer Simul 19:3086–3097
34. Nellis G, Klein S (2009) Heat transfer. Cambridge University Press, New York, USA, p E23–5
35. Lienhard JH IV, Lienhard JH V (2005) A heat transfer text book, 3rd edn. Phlogiston Press, Cambridge, pp 662–663
36. Uddin J, Kabir MN, Bég OA (2016) Computational investigation of Stefan blowing and multiple-slip effects on buoyancy-driven bioconvection nanofluid flow with microorganisms. Int J Heat Mass Transf 95:116–130
37. Buongiorno J (2006) Convective transport in nanofluids. J Heat Transf 128:240
38. Garoosi F, Garoosi S, Hooman K (2014) Numerical simulation of natural convection and mixed convection of the nano fluid in a square cavity using Buongiorno model. Powder Technol 268:279–292
39. Garoosi F, Jahanshaloo L, Garoosi S (2015) Numerical simulation of mixed convection of the nano fluid in heat exchangers using a Buongiorno model. Powder Technol 269:296–311
40. Malvandi A, Moshizi SA, Ghadam E, Ganji DD (2014) Modified Buongiorno' s model for fully developed mixed convection flow of nanofluids in a vertical annular pipe. Comput Fluids 89:124–132
41. Garoosi F, Jahanshaloo L, Rashidi MM, Badakhsh A, Ali ME (2015) Numerical simulation of natural convection of the nanofluid in heat exchangers using a Buongiorno model. Appl Math Comput 254:183–203
42. Sheremet MA, Pop I (2015) Mixed convection in a lid-driven square cavity filled by a nanofluid: Buongiorno' s mathematical model. Appl Math Comput 266:792–808
43. Sheremet MA, Pop I, Shenoy A (2015) Unsteady free convection in a porous open wavy cavity filled with a nanofluid using Buongiorno's mathematical model. Int Commun Heat Mass Transf 67:66–72

44. Tham L, Nazar R, Pop I (2014) Mixed convection flow from a horizontal circular cylinder embedded in a porous medium filled by a nanofluid: Buongiorno–Darcy model. Int J Therm Sci 84:21–33
45. Sheremet MA, Pop I (2014) Conjugate natural convection in a square porous cavity filled by a nanofluid using Buongiorno's mathematical model. Int J Heat Mass Transf 79:137–145
46. Sheremet MA, Pop I (2015) Free convection in a triangular cavity filled with a porous medium saturated by a nanofluid. Int J Numer Methods Heat Fluid Flow 25:1138–1161
47. Noghrehabadi A, Behseresht A, Ghalambaz M, Behseresht J (2013) Natural-convection flow of nanofluids over vertical cone embedded in non-Darcy porous media. J Thermophys Heat Transf 27:334–341
48. Rashidi MM, Momoniat E, Ferdows M, Basiriparsa A (2014) Lie group solution for free convective flow of a nanofluid past a chemically reacting horizontal plate in a porous media. Math Probl Eng 2014:1–21
49. Todd L (1997) A family of laminar boundary layers along a semi-infinite flat plate. Fluid Dyn Res 19:235–249
50. Fang T (2008) A note on the unsteady boundary layers over a flat plate. Int J Non Linear Mech 43:1007–1011
51. Rosca NC, Pop I (2014) Unsteady boundary layer flow of a nanofluid past a moving surface in an external uniform free stream using Buongiorno's model. Comput Fluids 95:49–55
52. Kuznetsov AV (2010) The onset of nanofluid bioconvection in a suspension containing both nanoparticles and gyrotactic microorganisms. Int Commun Heat Mass Transf 37:1421–1425
53. Stewartson K (2008) On the motion of a flat plate at high speed in a viscous compressible fluid. I. Impulsive motion. Math Proc Camb Philos Soc 51:202
54. Aziz A, Khan WA, Pop I (2012) Free convection boundary layer flow past a horizontal flat plate embedded in porous medium filled by nanofluid containing gyrotactic microorganisms. Int J Therm Sci 56:48–57
55. Anoop KB, Sundararajan T, Das SK (2009) Effect of particle size on the convective heat transfer in nanofluid in the developing region. Int J Heat Mass Transf 52:2189–2195
56. Javed T, Mehmood Z, Abbas Z (2017) Natural convection in square cavity filled with ferrofluid saturated porous medium in the presence of uniform magnetic field. Phys B Condens Matter 506:122–132
57. Javed T, Mehmood Z, Siddiqui MA, Pop I (2017) Effects of uniform magnetic field on the natural convection of Cu–water nanofluid in a triangular cavity. Int J Numer Methods Heat Fluid Flow 27:334–357
58. Javed T, Siddiqui MA, Mehmood Z, Pop I (2015) MHD natural convective flow in an isosceles triangular cavity filled with porous medium due to uniform/non-uniform heated side walls. Zeitschrift fur Naturforsch Sect A J Phys Sci 70:919–928